RESEARCH ARTICLE

Key Points:
- ICMEs can be grouped into three types as isolated ICME, multiple ICMEs, and shock ICMEs; multiple ICMEs mainly appeared in solar maximum
- About 58% ICME groups caused geomagnetic storms, while 20% caused intense storms; 87% intense geomagnetic storms were caused by ICME groups
- Shock-ICMEs are important sources of intense storms; the main effect is the shock compression on the south component of the magnetic field

Supporting Information:
- Table S1

Correspondence to:
C. Shen,
clshen@ustc.edu.cn

Statistical comparison of the ICME's geoeffectiveness of different types and different solar phases from 1995 to 2014

Chenglong Shen[1,2,3], Yutian Chi[1], Yuming Wang[1,2] [ID], Mengjiao Xu[1], and Shui Wang[1,4]

[1]CAS Key Laboratory of Geospace Environment, Department of Geophysics and Planetary Sciences, University of Science and Technology of China, Hefei, China, [2]Synergetic Innovation Center of Quantum Information and Quantum Physics, University of Science and Technology of China, Hefei, China, [3]Collaborative Innovation Center of Astronautical Science and Technology, Hefei, China, [4]Mengcheng National Geophysical Observatory, School of Earth and Space Sciences, University of Science and Technology of China, Hefei, China

Abstract The geoeffectiveness of interplanetary coronal mass ejections (ICMEs) is an important issue in space weather research and forecasting. Based on the ICME catalog that we recently established and the *Dst* indices from the World Data Center, we study and compare the geoeffectiveness of ICMEs of different in situ signatures and different solar phases from 1995 to 2014. According to different in situ signatures, all ICMEs are divided into three types: isolated ICMEs (I-ICMEs), multiple ICMEs (M-ICMEs), and shock-embedded ICMEs (S-ICMEs), resulting in a total of 363 group events. The main findings of this work are as follows: (1) Fifty-eight percent of ICMEs caused geomagnetic storms with $Dst_{min} \leq -30$ nT. Further, large fraction (87%) of intense geomagnetic storms are caused by ICME groups and their sheath regions. (2) Numbers of ICME groups and the probabilities of ICME groups in causing geomagnetic storms varied in pace with the solar cycle. Meanwhile, the ICME groups and the probabilities of them in causing geomagnetic storms in Solar Cycle 24 are much lower than those in Solar Cycle 23. (3) The maximum value of the intensity of the magnetic field (B), south component of the magnetic field (B_s), and dawn-dusk electric field vB_s are well correlated with the intensity of the magnetic storms. (4) Shock-embedded ICMEs have a high probability in causing geomagnetic storms, especially intense geomagnetic storms. (5) The compression of shock on the south component of magnetic field is an important factor to enhance the geoeffectiveness of S-ICMEs structures.

1. Introduction

Geomagnetic storms, which obviously influence the communication and the electric power transmission systems, are mainly caused by the coupling between the interplanetary magnetic field and magnetosphere. The magnetic reconnection between the south component of the interplanetary magnetic field and the magnetosphere is the main mechanism of such coupling [e.g., *Dungey*, 1961; *Gonzalez et al.*, 1994, 1999]. The interplanetary coronal mass ejections (ICMEs), which are the main carriers of the intense south component of the interplanetary magnetic field, are thought to be the main source of the geomagnetic storms especially for the intense geomagnetic storms [e.g., *Xue et al.*, 2005; *Yermolaev and Yermolaev*, 2006; *Gopalswamy*, 2006; *Gonzalez et al.*, 2007; *Zhang et al.*, 2007; *Echer et al.*, 2008; *Wu and Lepping*, 2008; *Richardson and Cane*, 2010; *Gonzalez et al.*, 2011; *Yermolaev et al.*, 2012; *Wu et al.*, 2013; *Wu and Lepping*, 2016; *Yermolaev et al.*, 2014; *Lawrance et al.*, 2016, and reference therein]. Most of these results indicate that large fraction of geomagnetic storms especially intense geomagnetic storms were caused by the ICMEs and their related structures.

If a slow CME and a fast CME successively erupted from the Sun at close location, the following fast CME will catch up and interact with the proceeding slow CME during their propagation in interplanetary space. The direct signature of such interaction was first reported by *Gopalswamy et al.* [2001] based on the radio spectrum observations from Wind. Now using the remote and multiple points observations from the Solar Terrestrial Relations Observatory (STEREO) [*Kaiser et al.*, 2008], the interaction between multiple CMEs can be traced and observed from their eruption to propagation arrival at the Earth. Using these observations, the kinematic evolution, the collision nature between multiple CMEs, and the radio signature of CME interaction have been

studied and discussed for some typical cases [e.g., *Shen et al.*, 2012; *Liu et al.*, 2012; *Temmer et al.*, 2012; *Lugaz et al.*, 2012, 2013; *Temmer et al.*, 2014; *Mishra et al.*, 2015; *Liu et al.*, 2014b, 2014a; *Colaninno and Vourlidas*, 2015; *Mishra et al.*, 2016].

When such interacted structures arrive at the Earth, the in situ measurements will show different signatures, such as the complex ejecta [*Burlaga et al.*, 2002], the multiple magnetic clouds (MCs) [*Wang et al.*, 2003a, 2005], the shock-embedded MC (shock-MC), or shock-embedded ICME (shock-ICME) events [*Ivanov*, 1982; *Lepping et al.*, 1997; *Wang et al.*, 2003b, 2003c; *Lugaz et al.*, 2015]. As the compression between multiple ICMEs or the shock and ICME would enhance the magnetic field intensity in the interaction structures, such events are thought to be more geoeffective than other events. *Lepping et al.* [1997] show an example that a possible shock propagated inside an MC. *Wang et al.* [2003c] reported that the shock-MC structure formed by fast forward shock overtaking preceding MC is an important cause of the large geomagnetic storms. *Xue et al.* [2005] analyzed eight great geomagnetic storms with $Dst_{min} \leq -200$ nT from 2000 to 2001 and found that four of them were caused by the compression between multiple CMEs. *Zhang et al.* [2007] found that 27% of intense geomagnetic storms with $Dst_{min} \leq -100$ nT from 1996 to 2005 were caused by multiple ICME interaction structures. Recently, *Lugaz et al.* [2015] statistically studied the shock inside ICMEs events and found that 19 out of 49 ICME-shock events in their study were associated with intense geomagnetic storms ($Dst_{min} \leq -100$ nT) within 12 h of the shock arrival at the Earth. All these results suggest that the multiple ICMEs especially the shock-ICMEs events are important factors in causing geomagnetic storms. But questions still remained, such as the following: (1) How significant can the interaction between multiple ICMEs, especially the shock-ICMEs, enhance their geoeffectiveness? (2) Is there any criteria under which CME interaction structure has enhanced geoeffectiveness?

Recently, we established an ICME catalog based on the plasma and magnetic field observations from the *Wind* spacecraft [*Chi et al.*, 2016]. The time coverage of this catalog is from 1996 to 2015. The criteria we used are as follows: (1) enhanced magnetic field intensity, (2) smoothly changing magnetic field direction, (3) declining profile of the solar wind velocity, (4) relatively low proton temperature to background solar wind, (5) relatively low proton plasma beta to background solar wind, and (6) bidirectional streaming of electrons. A structure is recognized as an ICME if it satisfies at least three of the criteria listed above, similar to our work in *Shen et al.* [2014]. In total, we identified 465 ICMEs during the study period. The online catalog of these ICMEs could be found at http://space.ustc.edu.cn/dreams/wind_icmes/. *Chi et al.* [2016] discussed the annual numbers of ICMEs, the annual numbers and ratios of MCs, the annual numbers of shocks driven by ICMEs, and the properties of ICMEs-, MCs-, ICME-driven shocks and the sheath regions. In addition, the solar cycle variations of these numbers and parameters have also been discussed.

As previously discussed, ICMEs, especially the multiple ICMEs, can exhibit different signatures in the in situ observations, such as isolated ICME, the complex structures, the multiple ICMEs, and the shock-ICME structures. The possible different geoeffectiveness of these different structures has also been reported in literature [e.g., *Wang et al.*, 2003, 2003c, 2003a; *Richardson and Cane*, 2004; *Xue et al.*, 2005; *Wu et al.*, 2006; *Gopalswamy*, 2006; *Zhang et al.*, 2007; *Richardson and Cane*, 2010; *Lugaz et al.*, 2015, and references therein]. In this paper, detailed analysis and comparison of the geoeffectiveness of ICMEs structures with different signatures will be shown. It should be noted that an interacted structure of the ICMEs will include more than one ICME. For these events, we treat all the ICMEs in an interacted structure as one group. Thus, all ICMEs in our list will be grouped and then divided into different types based on the in situ signatures. These groups are isolated ICMEs (I-ICMEs), multiple ICMEs (M-ICMEs), and shock-embedded ICMEs (S-ICMEs). The detailed definition of these ICMEs groups will be shown in section 2. It should be noted that the final or provisional *Dst* indices are not available for the year 2015. Thus, we will only study the ICMEs during the period from 1995 to 2014 in this work. The geoeffectiveness of all ICME groups will be discussed in section 3. In section 4, the comparison among the geoeffectiveness of the ICME groups in different types will be shown. In section 5, we will discuss the importance of the shock in enhancing the geoeffectiveness of ICMEs. Meanwhile, the criteria under which S-ICMEs had enhanced geoeffectiveness will also be discussed in this section. Finally, we will provide conclusions and some discussions.

2. Methods

As we discussed before, during its propagation from the Sun to the Earth, an ICME would probably interact with other ICMEs. Thus, the in situ observations of ICMEs always show different signatures. Possible types
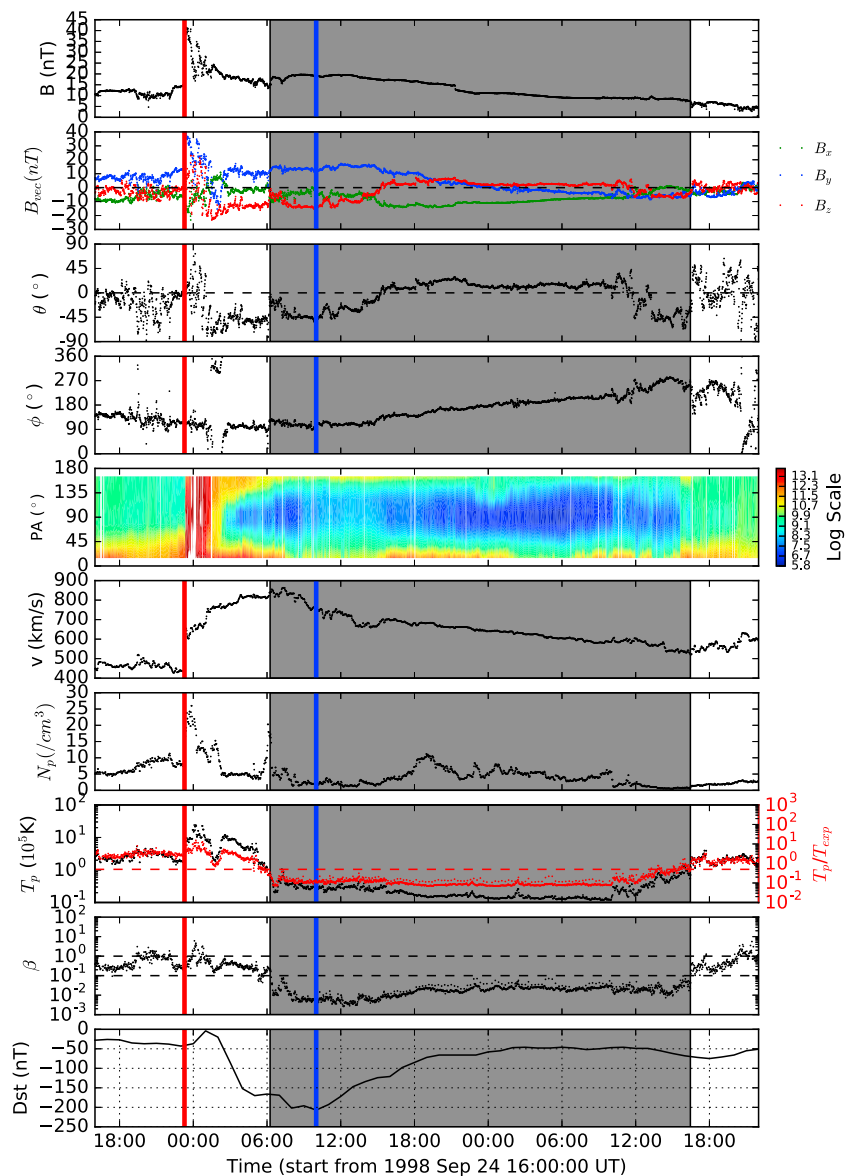
Figure 1. A typical example of the isolated ICME (I-ICME): 24–26 September 1998 event. From top to bottom, panels are the magnetic field strength (B), three components of the magnetic field in GSM coordinate system (B_x, B_y, and B_z), the elevation (θ) and azimuthal (ϕ) of magnetic field direction in GSM coordinate system, the suprathermal electron pitch angle distribution, solar wind speed (v), proton density (N_p), proton temperature (T_p) and the ratio of proton thermal pressure to magnetic pressure (β), and the Dst indices from WDC. The red vertical line shows the time of the shock driven by this ICME. The blue vertical line shows the peak time of the Dst index.

of ICMEs and interacted structures are isolated ICMEs, multiple ICMEs (or complex ejects) [*Burlaga et al.*, 2001; *Wang et al.*, 2003a], and shock-embedded ICMEs [*Ivanov*, 1982; *Lepping et al.*, 1997; *Wang et al.*, 2003b, 2003c; *Lugaz et al.*, 2015]. Thus, we group all ICMEs combined with their sheath regions in our list and then divide these groups into three types based on different in situ signatures.

1. *Type I: Isolated ICME (I-ICME)*. The simplest signature of ICME structure is isolated ICME. In this type, no interaction between multiple CMEs happen. Figure 1 shows a typical isolated ICME (I-ICME): the 24–26 September 1998 event. The shock driven by this ICME was first recorded at 23:17 UT 24 September 1998. After approximately 7 h, the main body of this ICME arrived at the Earth. Starting from 06:16 UT 25 September 1998 and ending at 16:27 UT 26 September 1998, the main body of this ICME took 34 h to pass through the Earth. During this period, the in situ observations show an obvious magnetic cloud (MC) structure with enhanced magnetic field intensity, large and smooth rotation of the magnetic field vector,
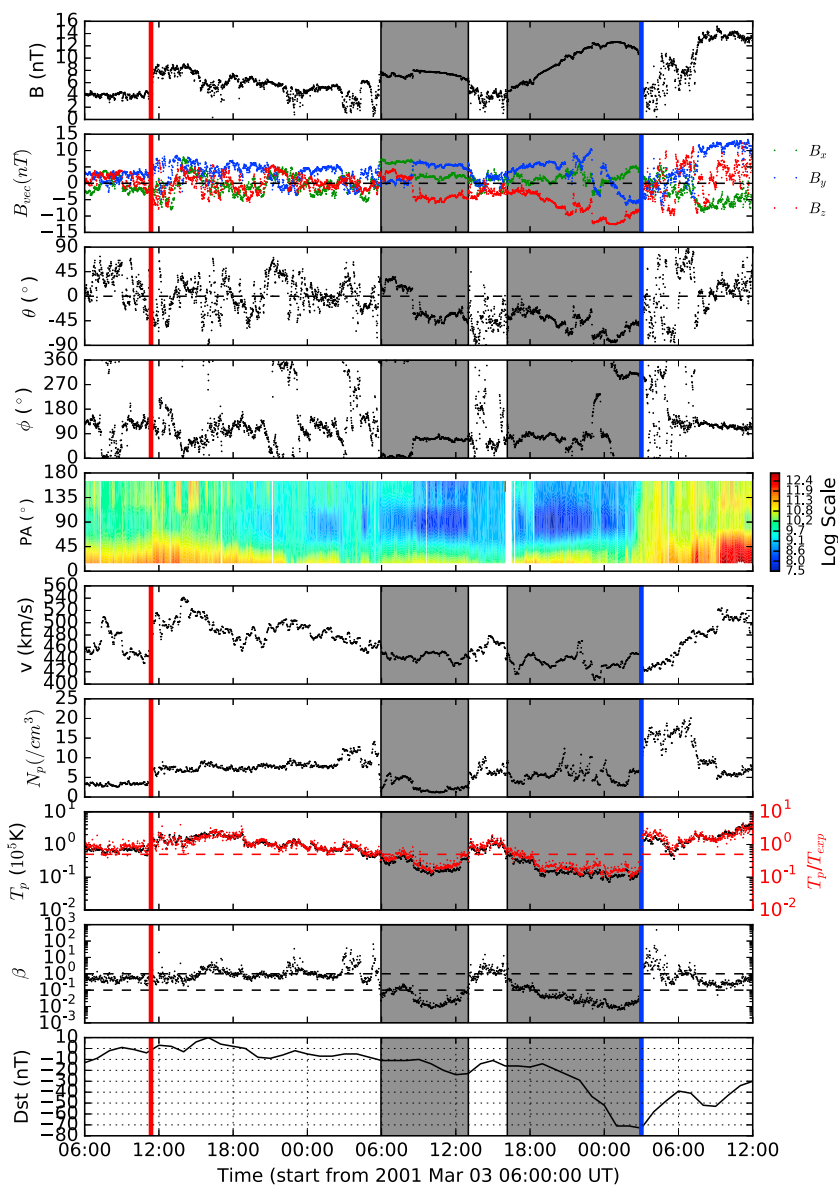
Figure 2. An example of the multiple ICMEs (M-ICMEs) interaction event: the 3 March 2001 event. The panels are the same as in Figure 1.

decreased velocity profile which may correspond to an expansion structure, low proton temperature, low proton plasma beta, and bidirectional electron streaming. This was a south-north (S-N)-type MC. The maximum value of B, B_s, v, and vB_s of this event are 41.5 nT, 23.2 nT, 863.2 km/s, and 17.2 mV/m, respectively. Meanwhile, 6 h before and after this ICME, no other ICME was recorded by *Wind*. Thus, this event is an I-ICME event. The bottom panel of Figure 1 shows the *Dst* index varied with time. It seems that this event caused an intense geomagnetic storm. The peak value of the *Dst* index of this storm (Dst_{min}) is −204 nT. This geomagnetic storm was caused by the south component of the magnetic field in the sheath region and MC region of this isolated ICME.

2. *Type II: Multiple-ICMEs (M-ICMEs) events*. In recent works, authors used the STEREO observations to track the interacted CMEs from the Sun to the Earth. In this work, there is no STEREO observation for most of the period we studied. Thus, we only use the in situ observations to find possible multiple-ICMEs (M-ICMEs) events. We define an M-ICMEs event as follows: ICMEs are grouped together as one M-ICMEs event if and only if the time interval between ICMEs is less than 6 h. Figure 2 shows an example of a typical M-ICMEs event: the 3 – 5 March 2001 event. This event, which is defined as a multiple magnetic clouds (MCs),
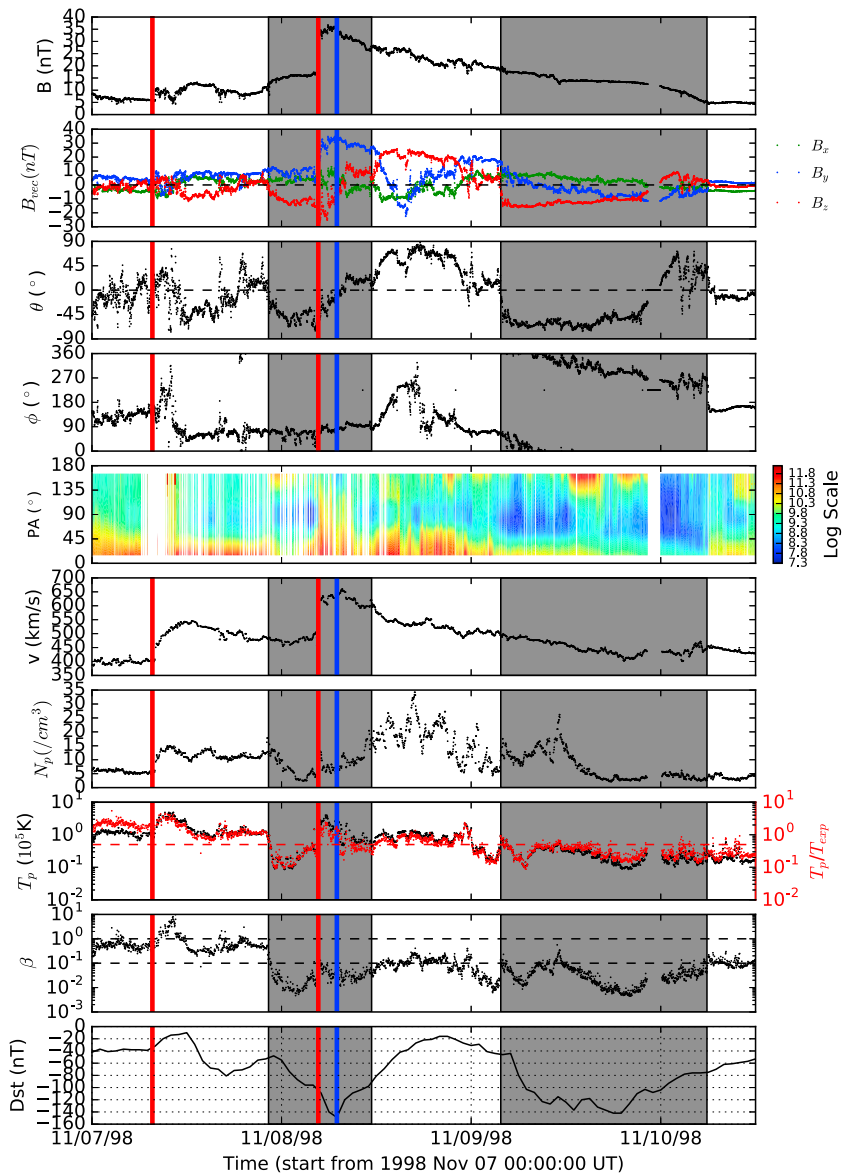
Figure 3. An example of the shock-ICMEs (S-ICMEs) interaction event: the 7 November 1998 event. The panels are the same as in Figure 1.

has been reported and studied by *Wang et al.* [2003a]. As the first gray region in Figure 2 shows, the first ICME was recorded from 05:06 UT 4 March 2001 to 13:01 UT 4 March 2001. After approximately 3 h, another ICME was detected by *Wind*. This ICME began at 16:10 UT 4 March 2001 and ended at 02:58 UT 5 March 2001. Between these two ICMEs, in situ observations show obvious interaction region signatures with low magnetic field intensity, enhanced proton number densities, and enhanced proton temperatures [*Wang et al.*, 2003a, 2005]. As seen from the last panel, this complex structure caused a geomagnetic storm with Dst_{min} of −73 nT. The peak time of this geomagnetic storm is 03:00 UT 5 March 2001.

It should be noted that in some cases, the shock driven by the following ICMEs will propagate into the preceding ICMEs. Thus, we can observe the shock-embedded ICMEs (S-ICMEs) structure near the Earth. Such events have been reported and studied by different authors [e.g., *Ivanov*, 1982; *Lepping et al.*, 1997; *Wang et al.*, 2003c; *Shen et al.*, 2008; *Lugaz et al.*, 2015]. Based on the definition of the M-ICMEs shown above, S-ICMEs structure is a special type of M-ICMEs. But considering the possible compression of the magnetic

Table 1. The Numbers and Percentages of ICME Groups in Different Types That Caused Different Geomagnetic Storms

	I-ICMEs	M-ICMEs	S-ICMEs	Total
All event	303 (84%)	22 (6%)	38 (10%)	363
Geomagnetic storms	164 (78%)	14 (7%)	33 (15%)	211
Weak geomagnetic storms	43 (82%)	5 (9%)	5 (9%)	53
Moderate geomagnetic storms	72 (86%)	6 (7%)	6 (7%)	84
Intense geomagnetic storms	49 (66%)	3 (4%)	22 (30%)	74

field by the shock inside the ICMEs, the geoeffectiveness of S-ICMEs may differ from other types of M-ICMEs. Thus, to check the different geoeffectiveness of these structure in detail, we divide the S-ICMEs event as a single type.

3. *Type III: Shock-embedded ICMEs (S-ICMEs) event*. In this type, a shock driven by a following ICME propagated into the ejecta region of the proceeding ICME. Figure 3 shows an example of the S-ICMEs event: the 7–10 November 1998 event. The gray shades show the regions of ICMEs. From 22:21 UT 7 November 1998 to 11:24 UT 8 November 1998 (the first gray shade), an ICME with an obvious magnetic cloud signature was recorded. The shock driven by this ICME arrived at the *Wind* ~ 15 h earlier at the time of 07:38 UT 7 November 1998. While the first ICME was passing through, another shock (as the red vertical solid line shows) was detected at 04:39 UT 8 November 1998. This means that this shock propagated into the ejecta of the first ICME. This shock compressed the first ICME, which obviously enhanced the strength of the magnetic field, the solar wind velocity, the proton number density, and the proton temperature of the first ICME. The maximum values of B, B_s, and vB_s in this MC are 36.8 nT, 660 km/s, and 27.8 nT and 16.3 mV/m, respectively. All these maximum values are located in the shock-compressed region of the first ICME. This S-ICMEs structure was associated with an intense geomagnetic storm with Dst_{min} of −149 nT soon after the arrival of the second shock. The second ICME, which we believe drove the second shock, arrived at the Earth at 03:45 UT 9 November 1998. After the arrival of the second ICME, another geomagnetic storm with Dst_{min} of −142 nT was recorded. This geomagnetic storm is mainly caused by the B_s carried by the ejecta of this ICME. In this work, to compare with other ICME groups, we only choose the largest one with $Dst_{min} = -149$ nT as the intensity of the geomagnetic storm caused by this S-ICMEs event.

As discussed above, in the events whose types are "S-ICMEs" or "M-ICMEs," there are at least two ICMEs and possibly more than two ICMEs. In this work, we treat all ICMEs in one event as a group. For example, in the 7 November 1998 S-ICMEs event, there are two ICMEs and we call them a S-ICMEs group. Based on the
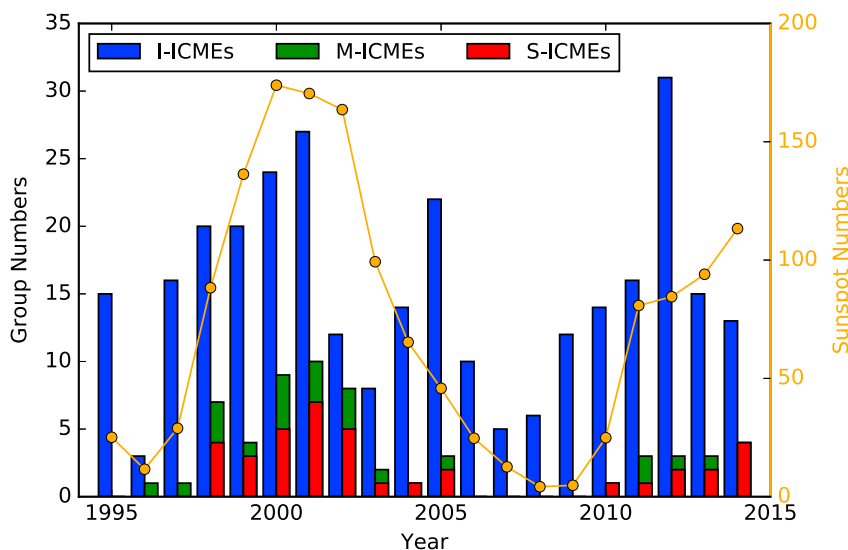
Figure 4. The annual number of the ICME groups in different types and the annual average sunspot numbers from 1995 to 2014. Blue bars show the numbers of I-ICME groups, and green and red bars show the number of M-ICMEs and S-ICMEs groups. The orange circles with solid line show the annual average sunspot numbers.

criteria above, all 436 ICMEs from 1995 to 2014 have been grouped and then divided into three different types. In total, we have 363 groups. The first column in the supporting information table shows the order number of each group, and the second column shows the type of each group. The capital letters "I," "M," and "S" indicate I-ICME, M-ICMEs, and S-ICMEs, respectively. The first column of Table 1 gives the numbers of ICME groups in different types. It demonstrates that the bulk of the ICME groups are I-ICME events (303 of 363: 84%), 22 (6%) are M-ICME events, and 38 (10%) are S-ICME events.

Figure 4 shows the annual number of ICME groups in different types. It can been seen in Figure 4 that a large fraction of M-ICMEs and S-ICMEs events occurred near the sunspot maximum. Eight (90%) M-ICMEs and 33 (87%) S-ICMEs occurred during the period from 1998 to 2003 and after 2011. The numbers of M-ICMEs and S-ICMEs in sunspot minimum are rare. Especially, no M-ICMEs or S-ICMEs groups were recorded at 1 AU in the extremely sunspot minimum from 2006 to 2009. This could be explained by the fact that near the sunspot maximum, the number of CMEs became larger. During the sunspot maximum, approximately six CMEs per day erupted from the Sun, whereas, less than one CME erupted from the Sun per day at the sunspot minimum [e.g., *Gopalswamy et al.*, 2015b]. Thus, CMEs have probably more to catch up with other CMEs and then form complex structures such as M-ICMEs or S-ICMEs at sunspot maximum.

3. Geoeffectiveness of ICME Groups

Dst indices from World Data Center (WDC) (http://wdc.kugi.kyoto-u.ac.jp/dstdir/index.html) are used to determine whether there was a geomagnetic storm associated with an ICME group. In this work, we associate a storm with an ICME group based on the following conditions: (1) the main phase of the geomagnetic storm is associated with the ICME group and (2) the peak time of the geomagnetic storm is close to the end time of the ICME group. Meanwhile, no other structure followed by the ICME group contributed to the main phase of this geomagnetic storm. If the peak value of the *Dst* indices (Dst_{min}) associated with an ICME group is equal or less than -30 nT, we say that this ICME group causes a geomagnetic storm. The third and fourth columns in the supporting information table show the time and values of peak *Dst* indices (Dst_{min}) for the geomagnetic storms associated with these ICME groups. The symbols "— —" indicate that no geomagnetic storm is associated with these ICME groups.

As the second column in Table 1 shows, all 363 ICME groups caused 211 geomagnetic storms with $Dst_{min} \leq -30$ nT. Thus, 58% of the ICME groups caused geomagnetic storms. Based on the definition of *Gonzalez et al.* [1994], we divide the geomagnetic storms into three types as follows: weak storm ($-50 < Dst_{min} \leq -30$ nT), moderate storm ($-100 < Dst_{min} \leq -50$ nT), and intense storm ($Dst_{min} \leq -100$ nT)). Totally, the ICME groups caused 53 weak storms, 84 moderate storms, and 74 intense geomagnetic storms. Large fractions (75%) of the geomagnetic storms caused by ICME groups are moderate and intense geomagnetic storms. Previous results show that the magnetic cloud (MCs) are more likely to cause geomagnetic storms [e.g., *Wu and Lepping*, 2016]. In this analysis, we treat the ICME groups as MC groups when at least one ICME in this group is MC. We totally have 143 MC groups. It means that about 39% ICME groups are MC groups. In the MC groups, about 74% caused geomagnetic storms which is much higher than the value of 48% for non-MC groups. This confirms the previous results.
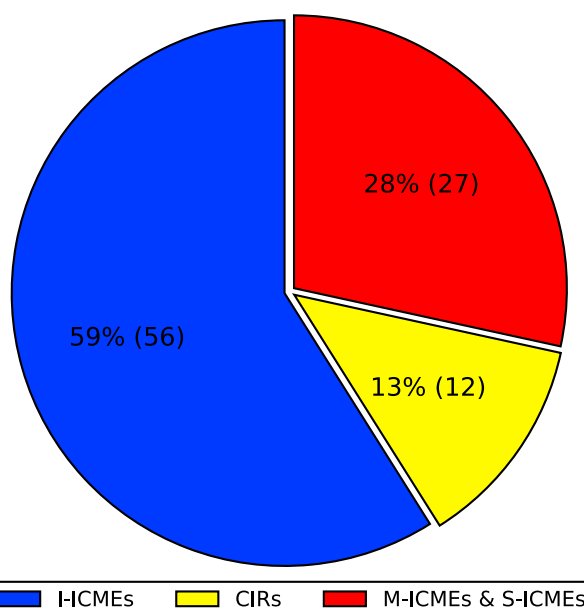
In previous works, the interplanetary origin of moderate and intense storms was studied by different authors for different time periods [e.g., *Gonzalez et al.*, 2007; *Zhang et al.*, 2007; *Echer et al.*, 2008, 2013]. In this work, the interplanetary origins of intense storms from 1995 to 2014 have been checked. Figure 5 shows the hourly average *Dst* indices from 1995 to 2014. Each diamond in this figure shows a geomagnetic storm event caused by an ICME group. By checking the *Dst* index month by month, we found that there are 21 intense geomagnetic storms that were not included in our list. By checking the in situ observations, we found that 12 of them were caused by the corotating interaction regions (CIRs) structures. In addition, the *Wind* observations for other nine events were not good enough to check the possible interplanetary drivers. Based on the intense geomagnetic storm list compiled by *Zhang et al.* [2007] and the in situ observations, the other nine events were possibly caused by ICMEs and their complex structures. Thus, we treat the drivers of these intense geomagnetic storms as ICMEs. And two of them were multiple-ICME events based on *Zhang et al.* [2007]. Totally, there are 56 intense geomagnetic storms caused by I-ICMEs and 27 events caused by multiple ICMEs (M-ICMEs and S-ICMEs). Another 12 intense geomagnetic storm events were caused by CIRs. The black circles in Figure 5 show the events caused by CIRs. Figure 6 shows the proportions of the interplanetary causes of intense geomagnetic storms. As seen from Figure 6, 59% of them was caused by the I-ICME and 28% was caused
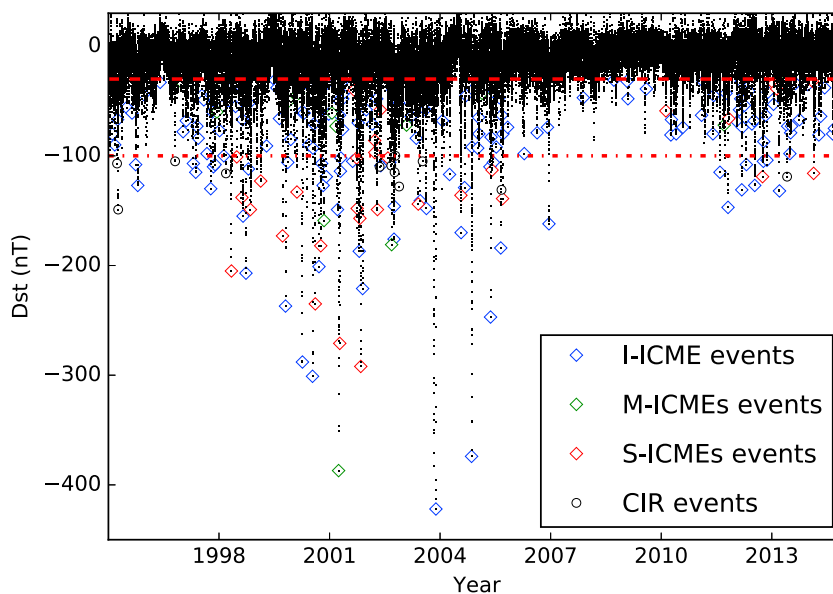
Figure 5. Dst indices from 1995 to 2014. All points in this panel are 1 h Dst indices, and only peaks are shown as diamonds. Dashed and dash-dotted horizontal lines show the criteria of $Dst = -30$ nT and $Dst = -100$ nT, respectively. Diamonds in different colors show the geomagnetic storms caused by different ICME groups. Blue, green, and red symbols show the events caused by I-ICME, M-ICMEs, and S-ICMEs groups, respectively. The black hollow circles show the intense geomagnetic storm events with $Dst_{min} \leq -100$ nT, which were not caused by ICME groups.

by the complex structures such as M-ICMEs and S-ICMEs. Meanwhile, another 13% intense geomagnetic storms were caused by CIRs. These ratios are the same as the result obtained by *Zhang et al.* [2007], who studied the solar and interplanetary sources of the intense geomagnetic storms with $Dst_{min} \leq -100$ nT from 1996 to 2005.

It should be noted that there are some geomagnetic storms only caused by the sheath regions driven by ICMEs. In our work, it is hard to check whether the geomagnetic storm is caused by sheath region only for M-ICMEs and S-ICMEs groups. For I-ICME groups, we find that 34 (20%) geomagnetic storms were only caused by the sheath regions driven by the ICMEs. In which, 10 (14%) moderate and 14 (29%) intense geomagnetic storms were only caused by the sheath region driven by the ICMEs. The ratio for intense storms is similar with the result (24%) obtained by *Gonzalez et al.* [2007] for intense geomagnetic storms during 1997–2005. But it is smaller than the result obtained by *Echer et al.* [2008] for superintense storms with $Dst_{min} \leq -250$ nT. A possible reason is that we exclude the S-ICMEs groups, in which the shock sheath region is an important cause of the geomagnetic storm. Another possible reason is that the main body of the ICMEs can easily cause geomagnetic storm with $Dst_{min} > -250$ nT. For moderate storm, the result we obtained is similar to the result of *Echer et al.* [2013] that 10.8% of moderate storms were caused by the sheath region only.

Figure 6. Proportions of the interplanetary causes of intense geomagnetic storms with $Dst_{min} \leq -100$ nT.
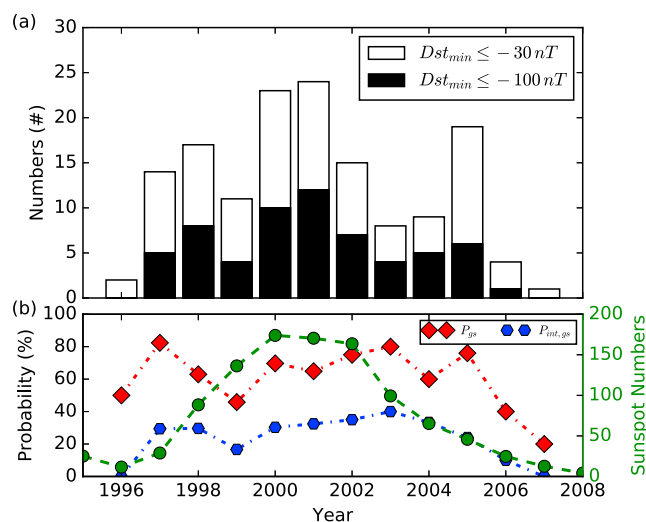
Figure 7. The solar cycle variation of the annual numbers of geomagnetic storms caused by ICME groups in Solar Cycle 23. (a) White bars and black bars show the annual numbers of geomagnetic storms and intense geomagnetic storms caused in ICME groups. (b) Red and blue lines and symbols show the probabilities of ICME groups in causing geomagnetic storms (P_{gs}) and intense geomagnetic storms ($P_{int,gs}$). The green line and symbols in Figure 7b show the sunspot numbers.

4. Solar Cycle Variation and Comparison Between Different Solar Cycles

Our list covers the full period of Solar Cycle 23. Thus, the solar cycle variation of the geoeffectiveness of ICME groups could be discussed. Figure 7a shows the annual numbers of geomagnetic storms in the whole period of Solar Cycle 23. Black bars show the numbers of intense geomagnetic storms. It is obvious that numbers of geomagnetic storms and intense geomagnetic storms varied in pace with sunspot numbers. In the rising phase, the annual numbers of geomagnetic storms caused by ICME groups increased with the increasement of sunspot numbers, while the annual numbers of geomagnetic storms caused by ICME groups decreased year by year in the declining phase. The numbers of geomagnetic storms in rising phase are higher than those in the declining phase. The correlation coefficient between the geomagnetic storm numbers and sunspot numbers is 0.71, while the correlation coefficient between the intense geomagnetic storm numbers and the sunspot numbers is 0.80. The red and blue lines in Figure 7b show the annual ratios of ICME groups in causing geomagnetic storms and intense geomagnetic storms. The annual ratios of ICME groups causing geomagnetic storm near solar maximum are higher than those in solar minimum. But the correlation coefficient between them and the sunspot numbers is very weak. Otherwise, the ratios of the ICME groups that caused intense geomagnetic storms are correlated with the sunspot numbers with correlation coefficient of 0.62. This result may show that not only the number of ICME groups but also the probability of ICME groups in causing geomagnetic storms are higher at solar maximum.

The extremely low geomagnetic activities in Solar Cycle 24 have been widely reported [e.g., *Jian et al.*, 2011; *Echer et al.*, 2011; *Richardson*, 2013; *Kilpua et al.*, 2014; *Gopalswamy et al.*, 2014; *Kilpua et al.*, 2014; *Gopalswamy et al.*, 2014; *Shi et al.*, 2014]. To make a better comparison, we choose two similar periods from Solar Cycles 23 and 24. The time range of the first period (period I) adopted from Solar Cycle 23 is 1 January 1996 to 31 December 2002. The second period (period II) from Solar Cycle 24 is 1 January 2008 to 31 December 2014. In period I of Solar Cycle 23, there are totally 212 ICMEs which formed 162 ICME groups. However, in the similar phase of Solar Cycle 24, the ICME number and ICME group number are larger than that in period I of Solar Cycle 23. The ICME number in period II is 137, about 35% smaller than that in period I. The ICME group number in period II is 121, about 25% smaller than in period I. It should be noted that the decrease of the group numbers in period II is smaller than the decrease of the ICME numbers. The reason is that the number of complex structure groups which may contain more than two ICMEs in period I is smaller than that in period II as Figure 4 showed.

In period I, ICME groups caused 106 geomagnetic storms with $Dst_{min} \leq -30$ nT and 46 geomagnetic storms with $Dst_{min} \leq -100$ nT. It means that in this period, there are 65% of the ICME groups that caused geomagnetic storm, while 28% of the ICMEs groups caused intense geomagnetic storms. All these values are higher than the values we obtained in section 3 for all the ICME groups. In period II, ICME groups only caused 56 geomagnetic storms in which only 10 events are intense geomagnetic storms. Thus, 46% and 8% of the ICME groups in period II caused geomagnetic storms and intense geomagnetic storms, respectively. Such numbers are much smaller than those in period I. These results indicate that in Solar Cycle 24, not only the ICMEs numbers but also the probabilities of ICMEs in causing geomagnetic storms are much smaller than those in Solar Cycle 23. The decrease of the ICMEs group number is caused by the lower solar activity in Solar Cycle 24
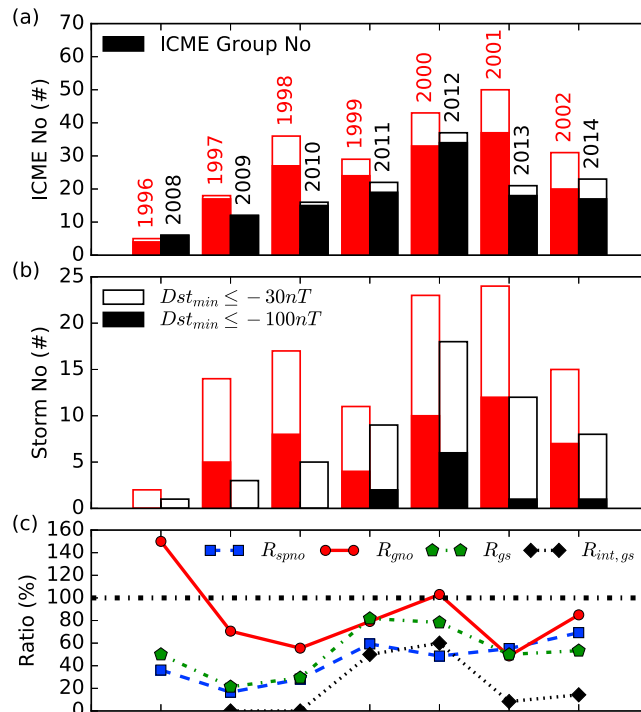
Figure 8. Comparison between similar period of Solar Cycles 23 and 24. (a) The ICME numbers (white bars) and ICME group numbers (red and black bars). Red and black color show the annual numbers from Solar Cycle 23 and 24, respectively. (b) The number of geomagnetic storms (white bars) and intense geomagnetic storms (red and black bars). (c) Different annual comparison ratios between two solar cycles. The blue (R_{spno}) and red (R_{gno}) lines in this panel show the annual comparison ratios of the sunspot numbers and ICME groups numbers between these two periods, respectively. Green (R_{gs}) and black ($R_{int,gs}$) lines show the yearly comparison ratios of the number of geomagnetic storms and intense geomagnetic storms between these two periods.

[e.g., *Gopalswamy et al.*, 2014; *Sun et al.*, 2015]. And the decrease of the possibility of ICMEs groups in causing geomagnetic storms might be caused by the lower magnetic field intensity in Solar Cycle 24 as shown in *Chi et al.* [2016] and other authors [e.g., *Jian et al.*, 2011; *Kilpua et al.*, 2012; *Gopalswamy et al.*, 2015a].

Figure 8 shows the detailed year by year comparison between period I (1996 to 2002) and period II (2008 to 2014). Bars in Figure 8a show the annual numbers of ICMEs and ICME groups. The red bars show the values in the years of Solar Cycle 23, while the white bars show the values in the years of Solar Cycle 24. The red and black bars show the numbers of ICME groups in these periods, respectively. It is obvious that the annual ICME numbers in Solar Cycle 23 are higher than those in Solar Cycle 24. As we discussed before, this might be caused by the fact that the solar activity in Solar Cycle 24 is much weaker than that in Solar Cycle 23 as the sunspot number variation has shown in Figure 4. The blue and red lines in Figure 8c show the annual comparison ratios $\left(= \frac{N_{24,Year}}{N_{23,Year}}\right)$ of the sunspot numbers and ICME groups numbers between these two periods. It is interesting that the decrease of the ICME group numbers is much larger than the decrease of sunspot numbers between these two periods. Similar result has also been reported by *Gopalswamy et al.* [2015b].
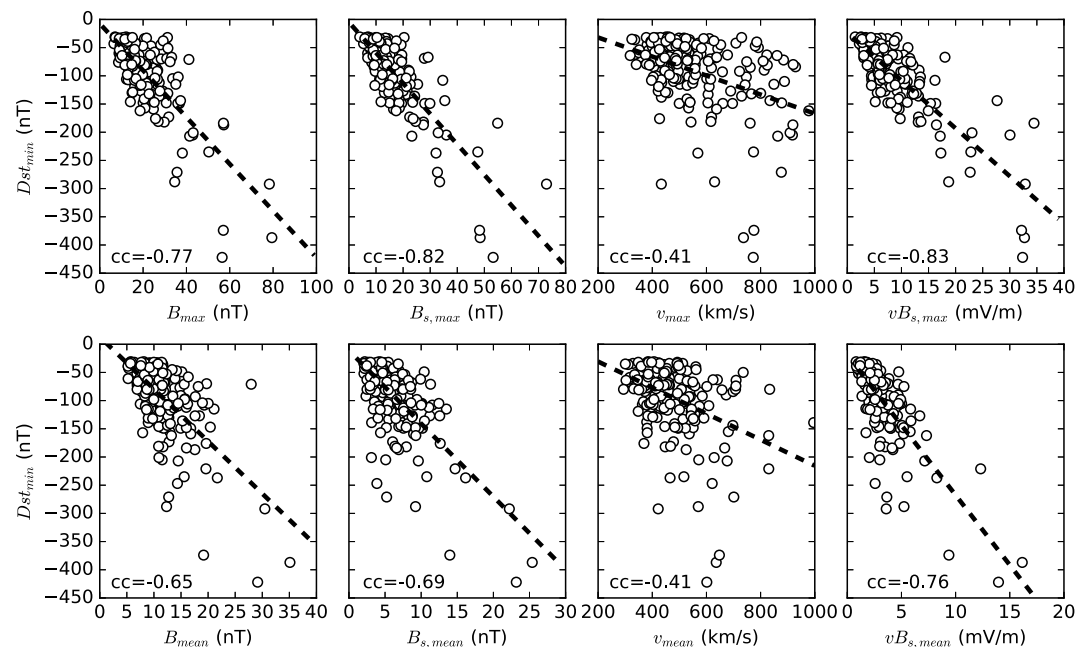
The bars in Figure 8b show the annual numbers of geomagnetic storms and intense geomagnetic storms in these two periods. Similar as the ICME numbers, the annual numbers of geomagnetic storms in Solar Cycle 24 are much smaller than those in Solar Cycle 23. Green and black lines in Figure 8c show the yearly comparison ratios of the number of geomagnetic storms and intense geomagnetic storms between these two periods. As seen from this panel, the trend of the annual comparison ratios between the geomagnetic storms is similar to the annual comparison ratio between sunspot numbers. But the annual comparison ratios of the intense geomagnetic storms are much smaller. One possible reason is that the number of strong ICMEs in Solar Cycle 24 is rare. Another possible reason is that the numbers of complex structures 24 are small in Solar Cycle 24.

5. Relationship Between ICME Parameters and the Intensity of the Geomagnetic Storms

To check the possible relationship between ICMEs' parameters and the intensity of the geomagnetic storms, correlation between ICME parameters and peak *Dst* was performed and results are shown in Figure 9. Figure 9 (top row) shows the scatter plots of ICMEs parameters and the intensity of the magnetic storms (Dst_{min}). From left to right, they show that Dst_{min} varied with B_{max}, $B_{s,max}$, v_{max}, and $vB_{s,max}$, respectively. It is found that the B_{max}, $B_{s,max}$, and $vB_{s,max}$ are well correlated with the Dst_{min}. The correlation coefficient between them are −0.77. −0.82, and −0.83, respectively. It confirms the result that the intensities of the geomagnetic storms

Figure 9. Scatter plots of ICME parameters with Dst_{min}. (top row) The correlation between the maximum values of ICMEs' parameters with Dst_{min}. (bottom row) The correlation between the mean values of ICMEs' parameters with Dst_{min}.

are controlled by the south component magnetic field or the dawn-dusk electric field. In previous works, the mean values of ICME parameters had also been used to study their correlation with Dst_{min}. Figure 9 (bottom row) shows the scatter plots of the mean parameters in ICME groups and Dst_{min}. Seen from these panels, the B_{mean}, $B_{s,mean}$, and $vB_{s,mean}$ are all also well correlated with the Dst_{min}. But the correlation coefficient are smaller than those for the maximum parameters. The correlation coefficients are −0.65, −0.69, and −0.75, respectively.

6. Comparison Between Different Group Types

Table 1 shows the proportions of different types of ICME groups for all events and geomagnetic storm events. As seen in Table 1, the proportions of the ICME groups that caused geomagnetic storms with $Dst_{min} \leq -30$ nT are similar to all ICME groups. But for the intense geomagnetic storms ($Dst_{min} \leq -100$ nT), the proportions of their source ICME groups are obviously different. Shown in the last row of Table 1, 30% of the intense storms with $Dst_{min} \leq -100$ nT were caused by S-ICMEs groups. It is much larger than the proportions for all ICME groups (10%), all geomagnetic storms(15%), weak geomagnetic storm (9%), and moderate geomagnetic storm (7%). This confirms the result that intense geomagnetic storms are more likely to be caused by S-ICMEs groups [e.g., *Wang et al.*, 2003c; *Xue et al.*, 2005; *Lugaz et al.*, 2015].

From another perspective, Figure 10 shows the probability of ICME groups to cause geomagnetic storms of different types. As seen from Figure 10, 58% ICME groups caused geomagnetic storms. Meanwhile, 15%, 23%, and 20% of them are weak, moderate, and intense geomagnetic storms, respectively. For I-ICME groups, these ratios are 54%, 14%, 24%, and 16% for all geomagnetic storms, weak geomagnetic storms, moderate geomagnetic storms, and intense geomagnetic storms, respectively. These values show the probability of I-ICME in causing different types of geomagnetic storms. We called them as $r_{i,gs}$, $r_{i,weak gs}$, $r_{i,mod gs}$, and $r_{i,int gs}$ hereafter. Symbols of "min," "mod," and "int" indicate the probability of one ICME in causing weak, moderate, and intense geomagnetic storms, respectively. For other groups of M-ICMEs and I-ICMEs, there are at least two ICMEs in each group. One can easily expect that one group with at least two isolated ICMEs can have higher probability to cause geomagnetic storm than one ICME even if no interaction happened. Thus, we can calculate the probability that two ICMEs can cause at least one geomagnetic storm based on the value of $r_{i,gs}$, $r_{i,weak gs}$, $r_{i,mod gs}$, and $r_{i,int gs}$ without the interaction effect between them. If the r is in unit of 100 which means that the r is the number of geomagnetic storms that can be caused by 100 I-ICMEs.
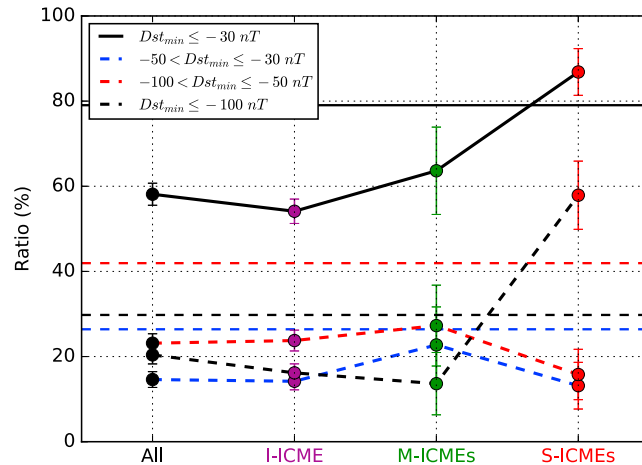
Figure 10. The ratio of the geoeffective ICMEs groups in different types. Error bars show 1 σ uncertainties calculated by $\sqrt{\frac{P(1-P)}{N}}$, where the P is the ratio while N is the total number of ICME groups in different types.

Thus, the probability of two ICMEs in causing geomagnetic storm is

$$r_{2CMEs} = 1 - \frac{C^1_{100-r}}{C^1_{100}}\frac{C^1_{99-r}}{C^1_{99}} \qquad (1)$$

Using the $r_{i,gs}$, we can get the probability of two ICMEs in causing at least one geomagnetic storms ($r_{2CMEs, gs}$). The calculated value of $r_{2CMEs, gs}$ is 78%. Meanwhile, the probabilities of two ICMEs in causing one weak storm, moderate storm, and intense storm are 26%, 42%, and 30%, respectively. The horizontal lines in Figure 10 show these values. The black solid horizontal line shows the $r_{2CMEs,gs}$ which is the possibility of 2 ICMEs in causing at least one geomagnetic storm. The blue, red, and black dash-dotted horizontal lines show the $r_{2CMEs,weak gs}$, $r_{2CMEs,mod gs}$, and $r_{2CMEs,int gs}$, respectively.

As seen from this figure, ratios of M-ICMEs groups to cause geomagnetic storms are little smaller than the expected values. It indicates that the simple interaction between multiple ICMEs do not enhance the geoeffectiveness of ICMEs obviously from statistical view. But, for S-ICMEs groups, the ratio in causing geomagnetic storms are significant larger than the calculated $r_{2CMES, gs}$. 87% S-ICMEs groups caused geomagnetic storms. This result strengthen the result that S-ICMEs events can cause geomagnetic storms easily from statistical view.

In addition, we also compare the different groups in causing different types of geomagnetic storms. The ratios of M-ICMEs groups are all smaller than the r_{2CMEs}. It further confirms the result that the simple interaction between multiple ICMEs do not enhance the geoeffectiveness of ICMEs. But for S-ICMEs groups, the ratio of them in causing intense geomagnetic storm is much higher than the calculated value of $r_{2CMEs, int gs}$. Meanwhile, ratios of S-ICMEs groups to cause weak and moderate geomagnetic storm are much lower than the calculated $r_{2CMEs,weak gs}$ and $r_{2CMEs, mod gs}$. This result confirms the observations that the shock compression magnetic storm can obviously enhance the geoeffectiveness of ICMEs. Thus, S-ICMEs are more likely to cause intense geomagnetic storms.

7. Geoeffectiveness of S-ICMEs Events

Previous results show that S-ICMEs can cause geomagnetic storms with higher possibility, 33 of the 38 S-ICMEs caused geomagnetic storms. But questions still remain: How significant is the effect of shock? Which shock can enhance the geoeffectiveness of ICMEs? To answer these questions, the S-ICMEs groups and their related structures are analyzed in detail. As we mentioned before, 33 S-ICMEs groups caused geomagnetic storms with $Dst_{min} \leq -30$ nT. Hereafter, we call these 33 groups as Geo-S-ICMEs groups. It should be noted that the most important factor in determining the geoeffectiveness of ICMEs is the south component of the magnetic field (B_s). If the shock propagated into a region in which magnetic fields are all northward, the compression of the shock could not obviously enhance the geoeffectiveness of ICMEs. By checking the in situ magnetic field observations for the other 5 S-ICMEs events, we found that these groups, which did not cause geomagnetic storms, did not carry or carried very weak south component of the magnetic field. This is the reason that these groups did not cause any geomagnetic storms with $Dst_{min} \leq -30$ nT.

By checking the in situ observations and the Dst indices of the Geo-S-ICMEs groups, we found that the main cause of the peak Dst intensity of the geomagnetic storms for these groups can be divided into four different types. Figure 11 shows the B_z (red lines) and Dst indices observations (black lines) for typical examples of these types. In each panel of Figure 11, the first gray-shaded region shows the period of preceding ICME in which a shock propagated. The blue vertical line shows the arrival time of inside shock. The second gray-shaded region shows the period of the following ICME which drove the shock.
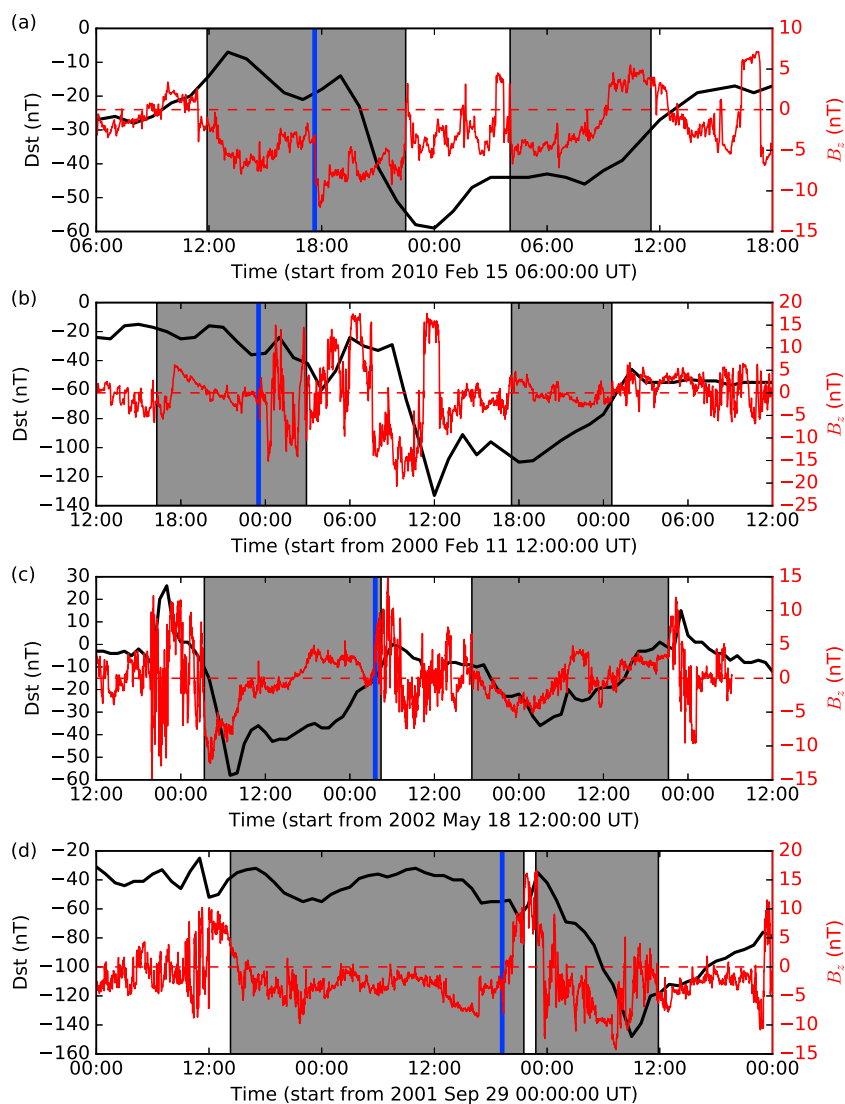
Figure 11. Typical examples of the different types of the causes of geomagnetic storms in S-ICMEs groups. Different panels show examples for different type S-ICMEs. The black line and red line show the *Dst* index and B_s, respectively. The shades show the periods of ICMEs and the blue vertical lines show the time of shock.

The detailed description of these four types are the following:

1. *Type I: Caused by the Shock Compressed Magnetic Field*. In this type, the peak *Dst* index of the geomagnetic storm is mainly caused by the shock-compressed magnetic field. Figure 11a shows an example of this type: 15 February 2010 S-ICMEs group. As seen from Figure 11a, this is an obviously two-step geomagnetic storm. The main phase of the first step of this geomagnetic storm started at 13:00 UT and reached its first minimum value (−21 nT) at the time of 15 February 2010 17:00 UT. After that, it began to recover. After about 30 min, the shock inside this ICME arrived at the Earth at 17:37 UT. This shock compressed the south component of the magnetic field obviously. With the arrival of this shock, the intensity of B_s jumped from ∼4 to ∼11 nT. After that, the second step of this geomagnetic storm started. About 6.5 h later, the *Dst* index reach its minimum value of −59 nT at the time of 16 February 2010 00:00 UT. Thus, for this event, the geomagnetic storm is mainly caused by the shock-compressed magnetic field. Totally, 15 Geo-S-ICMEs groups belong to this type and 12 of them caused intense geomagnetic storms. Meanwhile, 14 of these 15 geomagnetic storms show obvious two-step signature except the 25 September 2001 event. After checking the in situ observations, we found that no south component of the magnetic field was recorded by *Wind* before the shock arrival in the special event.

Table 2. The Number of S-ICMEs in Different Types That Caused Different Geomagnetic Storms

Types	I	II	III	IV
All storms	15 (46%)	4 (12%)	6 (18%)	8(24%)
Intense storms	12 (55%)	4 (18%)	2 (9%)	4 (18%)

2. *Type II: Caused by the interaction region between two ICMEs.* Figure 11b shows an example of this type: 11 February 2000 S-ICMEs event. This is another two-step geomagnetic storm. At the time of 12 February 2000 04:00 UT, the B_s carried by the first ICME caused the first step of the geomagnetic storm with the $Dst_{min} = -60$ nT. After that, this storm began to recover. After the arrival of the second ICME, the strong B_s in the interaction region between the two ICMEs, caused the second step of this intense geomagnetic storm. The Dst_{min} of this Geo-S-ICMEs group is -133 nT. Thus, this geomagnetic storm is mainly caused by the interaction region between two ICMEs. In this type, the most intense south components of the magnetic field are located in the interaction region between two ICMEs. Totally, four geomagnetic storms caused by S-ICMEs groups are this type.

3. *Type III: Caused by the preceding ICME.* Figure 11c shows an example: 18 May 2002 S-ICMEs event. As seen from Figure 11c, the geomagnetic storm of this event is mainly caused by the B_s carried by the first ICME. The B_s in the first ICME last from the arrival of this ICME to about 19 May 2002 14:00 UT. The shock was recorded by *Wind* at 20 May 2002 03:06 UT. The region that the shock passed through in the ICME are all northward magnetic field. Thus, the shock compression did not enhance the geoeffectiveness of this S-ICMEs event. In all Geo-S-ICMEs groups, six belong to this type.

4. *Type IV: Caused by the following ICMEs.* In this type, the geomagnetic storms are mainly caused by the B_s carried by the following ICMEs. Figure 11d shows an example: 29 September 2001 S-ICMEs group. In this event, the shock recorded by the *Wind* at 30 September 2001 19:13 UT, which is located at the rear boundary of this first ICME. The region passed through in the first ICME did not have obvious B_s. Meanwhile, B_s in the following ICME are much stronger than that in the first ICME. After the arrival of the second ICME, the *Dst* index decreased obviously. Thus, this geomagnetic storm was mainly caused by the following ICME. Totally, there are eight Geo-S-ICMEs groups in this type.

Table 2 lists the numbers and percentages of Geo-S-ICMEs groups in different types. As seen from this table, 46% of Geo-S-ICMEs is type I while 55% of Int-Geo-S-ICMEs is type I. It means that large fraction of Geo-S-ICMEs are in type I especially for intense geomagnetic storms. In addition, for all 15 events in type I, 12 of them were intense geomagnetic storms. It strengthens the result that the shock compression magnetic field can cause intense geomagnetic storm with higher possibility.

Previous results showed that not all shocks propagated into ICMEs can enhance their geoeffectiveness. One possible reason is that the shock did not propagate into the B_s region. In addition, to check whether the shock parameters would influence the geoeffectiveness, the parameters of these shocks propagated into ICMEs are obtained based on the Rankine-Hugoniot (R-H) analysis [e.g., *Viñas and Scudder*, 1986; *Szabo*, 1994; *Vorotnikov et al.*, 2008; *Koval and Szabo*, 2008]. Figures 12a and 12b show the scatter plots of these parameters. Red symbols show the events in type I while blue symbols show them in other types. As seen from these panels, the distribution of shock speed (v_{shock}), compression ratio, and the angle between shock normal and the upstream magnetic field vector θ_{Bn} for shocks in type I and other types are similar. In these shocks, inside ICMEs, 32 of them have well-established shock parameters. It is found that large fraction of them (29 of 32) are perpendicular shocks with $\theta_{Bn} \geq 45°$. This is as similar as the previous analysis for all interplanetary shocks [e.g., *Oliveira and Raeder*, 2015; *Chi et al.*, 2016]. *Echer et al.* [2006] and *Oliveira and Raeder* [2014] found that perpendicular shocks are more geoeffective. In our analysis, 14 of 29 perpendicular shocks inside ICME belong to type I. Otherwise, all the three parallel shocks are not in type I. It may confirm the result obtained by *Oliveira and Raeder* [2014]. But the sample number of the parallel shocks is too small to get a reliable result. However, the inside time (T_{inside}), which is defined as the time interval between the shock and the rear boundary of the ICME, exhibits obvious differences between type I and other types. The T_{inside} for shocks in type I is obviously longer than those in other types. To find possible critical shock T_{inside}, Figure 12c is obtained. Symbols in Figure 12c show the probabilities of the Geo-S-ICMEs events in type I when the inside time is smaller (red) or larger (black) than the critical time. As seen from Figure 12c, when the inside time is larger than 3 h, about 60% of Geo-S-ICMEs are type I events. While, no more than 20% Geo-S-ICMEs whose inside time are smaller than
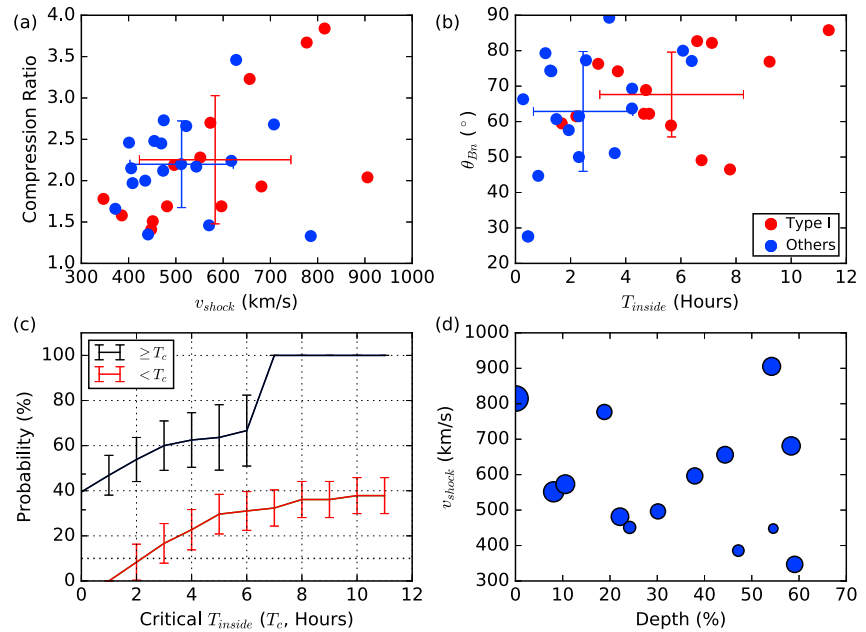
Figure 12. (a, b) The scatter plots of S-ICMEs groups shock parameters. Red symbols show the type I groups while other types are shown in blue. (c) The probabilities of S-ICMEs in type I when the T_{inside} is larger (black symbols) or smaller (red symbols) than the critical time (T_c). Error bars show 1 σ uncertainties calculated by $\sqrt{\frac{P(1-P)}{N}}$, where the P is the probability, while N is the total number. (d) The scatter plot of the shock speed with the related position of the shock. The size of symbol indicates the absolute value of the Dst_{min} for each group.

3 h are type I. Thus, 3 h is a possible critical time that the shock can enhance the geoeffectiveness of ICMEs. Possible reasons are as follows: (1) If the inside time is longer, the probability that the shock compressed the south component of the magnetic field became larger. (2) The longer inside time can make the shock well compress the magnetic field carried by ICMEs and enhance their geoeffectiveness. Meanwhile, *Wang et al.* [2003b] found that the higher overtaking shock speed and the deeper relative shock position in S-ICMEs group have more probability to cause intense geomagnetic storm. To check this result, Figure 12d is obtained. The *x* axis in Figure 12d shows the relative distance position (depth in unit of percentage) of the shock in the ICME. The value of 0 means the shock is located in the rear boundary, while the value of 100 means it is located in the front boundary. The sizes of these symbols show the relative intensity of the peak values of the *Dst* indices for these events. The larger the size is, the more intense the geomagnetic storm is. As seen from this panel, the intensity of the geomagnetic storms caused by these events seem to become larger from the lower left corner to upper right corner. Thus, it may confirm the result that the S-ICMEs group with the higher overtaking shock speed and the deeper relative shock position can cause more intense geomagnetic storm. But such tendency is not obvious enough. To get a more reliable result, more events should be analyzed further.

8. Discussion and Conclusion

In this work, the geoeffectiveness of different types of ICME groups from 1996 to 2014 has been studied and compared in detail. First, we grouped all ICMEs based on in situ observation signatures and then divided them into three types: I-ICME, M-ICMEs, and S-ICMEs. All 436 ICMEs in this period were placed in 363 groups, in which there are 303 I-ICME events, 22 M-ICMEs events, and 38 S-ICMEs events. Based on the statistical analysis of the geoeffectiveness of these ICME groups, we made the following conclusions:

1. Approximately 58% of ICME groups caused geomagnetic storms with $Dst_{min} \leq -30$ nT. For all the geomagnetic storms caused by ICMEs groups, there are 53 weak storms, 84 moderate storms, and 74 intense storms. Thus, large fraction (75%) of the geomagnetic storms caused by the ICME groups are moderated and intense storms. Meanwhile, almost all intense geomagnetic storms during the period we studied were caused by ICMEs.

2. The ICME number, ICME group number, and the probabilities of ICMEs in causing geomagnetic storms are well correlated with the sunspot number. It means that the numbers of ICME groups and also the

probabilities of ICME groups in causing geomagnetic storms varied in pace with the solar cycle. By comparing the geoeffectiveness of ICME group in Solar Cycles 23 and 24, we found that the ICME group number in Solar Cycle 24 is smaller than in Solar Cycle 23. In addition, the number of geomagnetic storms and also the probabilities of ICME groups in causing geomagnetic storms in Solar Cycle 24 are much lower than those in Solar Cycle 23.

3. The correlation between the ICMEs' parameters and the intensity of the magnetic storms (Dst_{min}) has also been discussed. We found that the mean and maximum values of the magnetic field (B), south component of the magnetic field (B_s), and dawn-dusk electric field vB_s are all well correlated with the Dst_{min}. It is consistent with the previous results about the correlation between ICMEs' parameters and Dst_{min} [e.g., *Wang et al.*, 2003; *Wu and Lepping*, 2016, and references therein]. The correlation coefficient between the maximum parameters in ICMEs and Dst_{min} are higher than the mean.

4. A large fraction of intense geomagnetic storms are caused by S-ICMEs interaction structures. Moreover, S-ICMEs complex structures can cause especially intense geomagnetic storms with high probability. The result that S-ICMEs interaction structures are important causes of geomagnetic storms has been reported and studied by *Wang et al.* [2003b, 2003c]. The reason is that the shock propagating into the preceding ICME would compress the magnetic field carried by them and increase the magnitudes of B_s, v, and $v_x B_s$ of ICMEs. In previous works, only a few cases were reported. This work shows the result that shock-embedded ICMEs are indeed important sources of geomagnetic storms especially intense ones in a statistical way. Recently, *Lugaz et al.* [2015] found that shocks propagating inside CMEs are one of the ways that strong B_s (and strong magnetic field) is created by compressing weak or average CMEs into CMEs with more extreme values in the magnetic field strength. Meanwhile, *Shen et al.* [2008] reported a definite case in which energetic particle intensities were enhanced in a S-ICMEs structure. They further found that such enhancement was the main cause of the largest solar energetic particle event in Solar Cycle 23. Combined with these results, we suggest that the S-ICMEs interaction structure is a very important factor in space weather forecasting.

It should be stressed that the most important parameter in determining the geoeffectiveness is the south component of the magnetic field carried by the ICMEs. Previous results show that the shock can intensify negative IMF B_z precondition by a factor of 3 to 6 [*Yue and Zong*, 2011]. For shock-ICMEs events, the shock compression also significantly enhanced the south component of the magnetic field in ICMEs. This is the main reason that the S-ICMEs can cause geomagnetic storms with higher probability.

It should be noted that CME cannibalism can make a single CME consisting of magnetic field lines and plasma from multiple CMEs [e.g., *Gopalswamy et al.*, 2001]. Recently, *Lugaz and Farrugia* [2014] reported an example of complex ejecta that might result from the interaction of two CMEs but show possible isolated ICME signatures. Only in situ observations are used in this work, which makes it hard to separate these ICMEs from isolated events. Moreover, there are some complex structures for which it is hard to distinguish whether they are isolated ICMEs or multiple ICMEs. Because of these facts, it is possible that there are some I-ICMEs in our list that should be M-ICMEs. This is a possible reason that the number of M-ICMEs events is small. In further work, the STEREO observations could be used to find the ICME interaction events from their large field view coronagraph observations. Thus, we can find the M-ICMEs events in a more accurate and similar way as *Lugaz and Farrugia* [2014] did.

References

Burlaga, L. F., R. M. Skoug, C. W. Smith, D. F. Webb, T. H. Zurbuchen, and A. Reinard (2001), Fast ejecta during the ascending phase of solar cycle 23: ACE observations, 1998–1999, *J. Geophys. Res.*, *106*(A), 20,957–20,978.

Burlaga, L. F., S. P. Plunkett, and O. C. St Cyr (2002), Successive CMEs and complex ejecta, *J. Geophys. Res.*, *107*(A), 1266, doi:10.1029/2001JA000255.

Chi, Y., C. Shen, Y. Wang, P. Ye, M. Xu, P. Ye, and S. Wang (2016), Statistical study of the interplanetary coronal mass ejections from 1995 to 2016, *Sol. Phys.*, *291*(8), 2419–2439, doi:10.1007/s11207-016-0971-5.

Colaninno, R. C., and A. Vourlidas (2015), Using multiple-viewpoint observations to determine the interaction of three coronal mass ejections observed on 2012 March 5, *Astrophys. J.*, *815*(1), 70, doi:10.1088/0004-637X/815/1/70.

Dungey, J. W. (1961), Interplanetary magnetic field and the auroral zones, *Phys. Rev. Lett.*, *6*(2), 47–48.

Echer, E., W. D. Gonzalez, and M. V. Alves (2006), On the geomagnetic effects of solar wind interplanetary magnetic structures, *Space Weather*, *4*, 1–11, doi:10.1029/2005SW000200.

Echer, E., W. D. Gonzalez, and B. T. Tsurutani (2008), Interplanetary conditions leading to superintense geomagnetic storms ($Dst \leq -250$ nT) during solar cycle 23, *Geophys. Res. Lett.*, *35*, L06S03, doi:10.1029/2008GL034731.

Echer, E., B. T. Tsurutani, and W. D. Gonzalez (2011), Extremely low geomagnetic activity during the recent deep solar cycle minimum, *Proc. Int. Astron. Union*, *7*(S286), 200–209, doi:10.1017/S174392131200484X.

Echer, E., B. T. Tsurutani, and W. D. Gonzalez (2013), Interplanetary origins of moderate (−100 nT < Dst ≤ − 50 nT) geomagnetic storms during solar cycle 23 (1996–2008), *J. Geophys. Res. Space Physics*, *118*, 385–392, doi:10.1029/2012JA018086.

Gonzalez, W., B. Tsurutani, and A. de Gonzalez (1999), Interplanetary origin of geomagnetic storms, *Space Sci. Rev.*, *88*, 529–562.

Gonzalez, W. D., J. A. Joselyn, Y. Kamide, H. W. Kroehl, G. Rostoker, B. T. Tsurutani, and V. M. Vasyliunas (1994), What is a geomagnetic storm?, *J. Geophys. Res.*, *99*(A4), 5771–5792.

Gonzalez, W. D., E. Echer, A. L. Clua-Gonzalez, and B. T. Tsurutani (2007), Interplanetary origin of intense geomagnetic storms (*Dst* < −100 nT) during solar cycle 23, *Geophys. Res. Lett.*, *34*, L06101, doi:10.1029/2006GL028879.

Gonzalez, W. D., E. Echer, B. T. Tsurutani, A. L. Gonzalez, and A. Lago (2011), Interplanetary origin of intense, superintense and extreme geomagnetic storms, *Space Sci. Rev.*, *158*(1), 69–89.

Gopalswamy, N. (2006), Properties of interplanetary coronal mass ejections, *Space Sci. Rev.*, *124*(1), 145–168.

Gopalswamy, N., S. Yashiro, M. L. Kaiser, R. A. Howard, and J. L. Bougeret (2001), Radio signatures of coronal mass ejection interaction: Coronal mass ejection cannibalism?, *Astrophys. J.*, *548*(1), L91–L94.

Gopalswamy, N., A. Lara, S. Yashiro, S. Nunes, and R. A. Howard (2003), Coronal mass ejection activity during solar cycle 23, in *Solar Variability as an Input to the Earth's Environment. International Solar Cycle Studies (ISCS) Symposium*, vol. 535, pp. 403–414, ESA Publ. Div., Noordwijk.

Gopalswamy, N., S. Akiyama, S. Yashiro, H. Xie, P. Mäkelä, and Grzegorz Michalek (2014), Anomalous expansion of coronal mass ejections during solar cycle 24 and its space weather implications, *Geophys. Res. Lett.*, *41*, 2673–2680, doi:10.1002/2014GL059858.

Gopalswamy, N., S. Yashiro, H. Xie, S. Akiyama, and P. Mäkelä (2015a), Properties and geoeffectiveness of magnetic clouds during solar cycles 23 and 24, *J. Geophys. Res. Space Physics*, *120*, 9221–9245, doi:10.1002/2015JA021446.

Gopalswamy, N., P. Mäkelä, S. Akiyama, S. Yashiro, and N. Thakur (2015b), CMEs during the two activity peaks in cycle 24 and their space weather consequences, *Sun Geosphere*, *10*(2), 111–118.

Ivanov, K. G. (1982), A study of some interplanetary shock wave tendencies, *Space Sci. Rev.*, *32*, 49–63, doi:10.1007/s13398-014-0173-7.2.

Jian, L. K., C. T. Russell, and J. G. Luhmann (2011), Comparing solar minimum 23/24 with historical solar wind records at 1 AU, *Sol. Phys.*, *274*(1-2), 321–344.

Kaiser, M. L., T. A. Kucera, J. M. Davila, O. C. St Cyr, M. Guhathakurta, and E. Christian (2008), The STEREO mission: An introduction, *Space Sci. Rev.*, *136*(1), 5–16.

Kilpua, E. K. J., L. K. Jian, Y. Li, J. G. Luhmann, and C. T. Russell (2012), Observations of ICMEs and ICME-like solar wind structures from 2007–2010 using Near-Earth and STEREO observations, *Sol. Phys.*, *281*, 391.

Kilpua, E. K. J., M. Mierla, A. N. Zhukov, L. Rodriguez, A. Vourlidas, and B. Wood (2014), Solar sources of interplanetary coronal mass ejections during the solar cycle 23/24 minimum, *Sol. Phys.*, *289*(10), 3773–3797, doi:10.1007/s11207-014-0552-4.

Koval, A., and A. Szabo (2008), Modified "Rankine-Hugoniot" shock fitting technique: Simultaneous solution for shock normal and speed, *J. Geophys. Res.*, *113*, A10110, doi:10.1029/2008JA013337.

Lawrance, M. B., A. Shanmugaraju, Y. J. Moon, M. S. Ibrahim, and S. Umapathy (2016), Relationships between interplanetary coronal mass ejection characteristics and geoeffectiveness in the rising phase of solar cycles 23 and 24, *Sol. Phys.*, *291*(5), 1547–1560, doi:10.1007/s11207-016-0911-4.

Lepping, R. P., et al. (1997), The Wind magnetic cloud and events of October 18–20, 1995: Interplanetary properties and as triggers for geomagnetic activity, *J. Geophys. Res.*, *102*, 14,049–14,063.

Liu, Y. D., et al. (2012), Interactions between coronal mass ejections viewed in coordinated imaging and in situ observations, *Astrophys. J. Lett.*, *746*(2), L15.

Liu, Y. D., Z. Yang, R. Wang, J. G. Luhmann, and J. D. Richardson (2014a), Sun-To-Earth characteristics of two coronal mass ejections interacting near 1 Au: Formation of a complex ejecta and generation of a two-step geomagnetic storm, *Astophys. J. Lett.*, *793*, L41, doi:10.1088/2041-8205/793/2/L41.

Liu, Y. D., Z. W. Yang, R. Wang, J. G. Luhmann, and J. D. Richardson (2014b), Observations of an extreme storm in interplanetary space caused by successive coronal mass ejections, *Nat. Commun.*, *5*, 3481, doi:10.1038/ncomms4481.

Lugaz, N., and C. J. Farrugia (2014), A new class of complex ejecta resulting from the interaction of two CMEs and its expected geoeffectiveness, *Geophys. Res. Lett.*, *41*, 769–776, doi:10.1002/2013GL058789.

Lugaz, N., C. J. Farrugia, J. A. Davies, C. Möstl, C. J. Davis, I. I. Roussev, and M. Temmer (2012), The deflection of the two interacting coronal mass ejections of 2010 May 23–24 as revealed by combined in situ measurements and heliospheric imaging, *Astrophys. J.*, *759*(1), 68.

Lugaz, N., C. J. Farrugia, W. B. Manchester IV, and N. Schwadron (2013), The interaction of two coronal mass ejections: Influence of relative orientation, *Astrophys. J.*, *778*(1), 20, doi:10.1088/0004-637X/778/1/20.

Lugaz, N., C. J. Farrugia, C. W. Smith, and K. Paulson (2015), Shocks inside CMEs: A survey of properties from 1997 to 2006, *J. Geophys. Res. Space Physics*, *23*, 2409–2427, doi:10.1002/2014JA020848.

Mishra, W., N. Srivastava, and D. Chakrabarty (2015), Evolution and consequences of interacting CMEs of 9–10 November 2012 using STEREO/SECCHI and in situ observations, *Sol. Phys.*, *290*(2), 527–552, doi:10.1007/s11207-014-0625-4.

Mishra, W., Y. Wang, and N. Srivastava (2016), On understanding the nature of collisions of coronal mass ejections observed by STEREO, *Astrophys. J.*, *831*(1), 99, doi:10.3847/0004-637X/831/1/99.

Oliveira, D. M., and J. Raeder (2014), Impact angle control of interplanetary shock geoeffectivenes, *J. Geophys. Res. Space Physics*, *119*, 8188–8201, doi:10.1002/2014JA020275.

Oliveira, D. M., and J. Raeder (2015), Impact angle control of interplanetary shock geoeffectiveness: A statistical study, *J. Geophys. Res. Space Physics*, *120*, 4313–4323, doi:10.1002/2015JA021147.

Richardson, I. G. (2013), Geomagnetic activity during the rising phase of solar cycle 24, *J. Space Weather Space Clim.*, *3*, A08, doi:10.1051/swsc/2013031.

Richardson, I. G., and H. V. Cane (2004), Identification of interplanetary coronal mass ejections at 1 AU using multiple solar wind plasma composition anomalies, *J. Geophys. Res.*, *109*, A09104, doi:10.1029/2004JA010598.

Richardson, I. G., and H. V. Cane (2010), Near-Earth interplanetary coronal mass ejections during solar cycle 23 (1996–2009): Catalog and summary of properties, *Sol. Phys.*, *264*, 189.

Shen, C., Y. Wang, P. Ye, and S. Wang (2008), Enhancement of solar energetic particles during a shock—Magnetic cloud interacting complex structure, *Sol. Phys.*, *252*(2), 409–418.

Shen, C., Y. M. Wang, S. Wang, Y. Liu, R. Liu, A. Vourlidas, B. Miao, P. Z. Ye, J. J. Liu, and Z. J. Zhou (2012), Super-elastic collision of large-scale magnetized plasmoids in the heliosphere, *Nat. Phys.*, *8*(1), 923–928.

Shen, C., Y. Wang, Z. Pan, B. Miao, P. Ye, and S. Wang (2014), Full-halo coronal mass ejections: Arrival at the Earth, *J. Geophys. Res. Space Physics*, *119*, 5107–5116, doi:10.1002/2014JA020001.

Shi, L. W., C. L. Shen, and Y. M. Wang (2014), The interplanetray origins of geomagnetic storm with $Dst < -50$ nT in 2007–2012, *Chin. J. Geophys. Chin. Edn.*, *57*(11), 3822–3833.

Sun, X. D., J. T. Hoeksema, Y. Liu, and J. W. Zhao (2015), On polar magnetic field reversal and surface flux transport during solar cycle 24, *Astrophys. J.*, *798*(2), 114.

Szabo, A. (1994), An improved solution to the Rankine-Hugoniot problem, *J. Geophys. Res.*, *99*(A8), 14,737–14,746.

Temmer, M., et al. (2012), Characteristics of kinematics of a coronal mass ejection during the 2010 August 1 CME-CME interaction event, *Astrophys. J.*, *749*(1), 57.

Temmer, M., A. M. Veronig, V. Peinhart, and B. Vršnak (2014), Asymmetry in the CME-CME interaction process for the events from 2011 February 14–15, *Astrophys. J.*, *785*(2), 85, doi:10.1088/0004-637X/785/2/85.

Vorotnikov, V. S., C. W. Smith, Q. Hu, A. Szabo, R. M. Skoug, and C. M. S. Cohen (2008), Automated shock detection and analysis algorithm for space weather application, *Space Weather*, *6*, 1–12, doi:10.1029/2007SW000358.

Viñas, A. F., and J. D. Scudder (1986), Fast and optimal solution to the Rankine-Hugoniot problem, *J. Geophys. Res.*, *91*(A1), 39–58.

Wang, Y., C. L. Shen, S. Wang, and P. Z. Ye (2003), An empirical formula relating the geomagnetic storm's intensity to the interplanetary parameters: $-VB_z$ and Δt, *Geophys. Res. Lett.*, *30*(20), 2039, doi:10.1029/2003GL017901.

Wang, Y., H. Zheng, S. Wang, and P. Ye (2005), MHD simulation of the formation and propagation of multiple magnetic clouds in the heliosphere, *Astron. Astrophys.*, *434*(1), 309–316.

Wang, Y. M., P. Z. Ye, and S. Wang (2003a), Multiple magnetic clouds: Several examples during March–April 2001, *J. Geophys. Res.*, *108*(A10), doi:10.1029/2003JA009850.

Wang, Y. M., P. Z. Ye, S. Wang, and M. Xiong (2003b), Theoretical analysis on the geoeffectiveness of a shock overtaking a preceding magnetic cloud, *Sol. Phys.*, *216*(1-2), 295–310, doi:10.1023/A:1026150630940.

Wang, Y. M., P. Z. Ye, S. Wang, and X. H. Xue (2003c), An interplanetary cause of large geomagnetic storms: Fast forward shock overtaking preceding magnetic cloud, *Geophys. Res. Lett.*, *30*(13), 1700, doi:10.1029/2002GL016861.

Wu, C. C., and R. P. Lepping (2008), Geomagnetic activity associated with magnetic clouds, magnetic cloud-like structures and interplanetary shocks for the period 1995–2003, *Adv. Space Res.*, *41*(2), 335–338, doi:10.1016/j.asr.2007.02.027.

Wu, C. C., and R. P. Lepping (2016), Relationships among geomagnetic storms, interplanetary shocks, magnetic clouds, and sunspot number during 1995–2012, *Sol. Phys.*, *291*(1), 265–284, doi:10.1007/s11207-015-0806-9.

Wu, C.-C., R. P. Lepping, and N. Gopalswamy (2006), Relationships among magnetic clouds, CMES, and geomagnetic storms, *Sol. Phys.*, *239*(1), 449–460.

Wu, C. C., N. Gopalswamy, R. P. Lepping, and S. Yashiro (2013), Characteristics of magnetic clouds and interplanetary coronal mass ejections which cause intense geomagnetic storms, *Terr. Atmos. Oceanic Sci.*, *24*(2), 233–241, doi:10.3319/TAO.2012.09.26.03(SEC).

Xue, X. H., Y. Wang, P. Z. Ye, S. Wang, and M. Xiong (2005), Analysis on the interplanetary causes of the great magnetic storms in solar maximum (2000–2001), *Planet. Space Sci.*, *53*(4), 443–457.

Yermolaev, Y., I. Lodkina, N. Nikolaeva, and M. Yermolaev (2014), Dependence of the durations of main and recovery phases of magnetic storms on the interplanetary driver type, *Geophys. Res. Abstr.*, *16*, EGU2014–5518, EGU General Assembly.

Yermolaev, Y. I., and M. Y. Yermolaev (2006), Statistic study on the geomagnetic storm effectiveness of solar and interplanetary events, *Adv. Space Res.*, *37*(6), 1175–1181.

Yermolaev, Y. I., N. S. Nikolaeva, I. G. Lodkina, and M. Y. Yermolaev (2012), Geoeffectiveness and efficiency of CIR, sheath, and ICME in generation of magnetic storms, *J. Geophys. Res.*, *117*(5), 1–9, doi:10.1029/2011JA017139.

Yue, C., and Q. Zong (2011), Solar wind parameters and geomagnetic indices for four different interplanetary shock/ICME structures, *J. Geophys. Res.*, *116*(12), 1–11, doi:10.1029/2011JA017013.

Zhang, J., et al. (2007), Solar and interplanetary sources of major geomagnetic storms ($Dst \leq -100$ nT) during 1996–2005, *J. Geophys. Res.*, *112*, A10102, doi:10.1029/2007JA012321.